Contributed paper

OPTO-ELECTRONICS REVIEW **11**(2), 161–167 (2003)

Spectral detectivity and NETD of doping-spike PtSi/p-Si and GeSi/Si HIP detectors

A.V. VOITSEKHOVSKII*, A.P. KOKHANENKO, and S.N. NESMELOV

Siberian Physico-Technical Institute, 1 Novosobornaya Av., 634050 Tomsk, Russia

Platinum silicide Schottky barrier detectors (SBD) and GeSi/Si-based heterojunction internal photoemission (HIP) detectors are widely used for application in the infrared spectral range. The increase in cutoff wavelength and responsivity of PtSi/Si photodevices is possible by formation of heavily-doped thin layer near to the semiconductor surface. The cutoff wavelength of Ge_xSi_{1-x}*/Si-based HIPdetectors depends on x and concentration of boron in GeSi.*

In this report, the threshold properties of these detectors are considered. The dependencies of spectral detectivities and NETD on cutoff wavelength are calculated for various parameters of SBD and HIP detectors. It is shown that optimal NETD of a SBD and HIP detectors is possible for certain cutoff wavelength and temperature of detectors and depends on storage capacity. Also opportunity of formation of heavily-doped nanolayer in SBD detectors used by short-pulse recoil implantation of boron was studied.

Keywords: PtSi/Si barrier, heavily-doped nanolayers, SBD detectors, HIP detectors, GeSi/Si heterojunctions.

1. Introduction

An important problem facing the developers of infrared Schottky barrier detectors (SBD) is to increase the quantum efficiency and extend the spectral range of the photodetector sensitivity to the long wavelength region. This can be achieved by reducing the potential metal-semiconductor barrier [1–5]. The potential barrier height can be varied by producing a thin highly-doped layer on the semiconductor surface. For example, it was proposed in Refs. 6–9 that the effective potential barrier can be reduced by producing on the semiconductor surface a thin layer which conduction type is the same as that of the semiconductor substrate. Formation of heavily-doped surface layers allows the cutoff wavelength of photodetectors to be increased and the quantum efficiency for a given wavelength to be improved.

The use of molecular-beam epitaxy (MBE) makes it possible to produce surface layers with a stepped distribution of a dopant about 1 nm thick [8,9]. The disadvantages of this method are high production cost of samples and complex technological cycle. Conventional ion implantation based on CW ion sources gives no way to attain the parameters required for the heavily-doped region. The recent development in the MBE technology made it possible to fabricate high quality Ge_xSi_{1-x} (GeSi) thin films onto silicon substrates and heterojunction internal photoemissive detectors in base of Ge_xSi_{1-x} were successfully developed [10,11]. The cutoff wavelength of HIP detectors depends on x and boron concentration in GeSi and varied from 3 to 23 µm.

In this work, we present experimental results about formation heavily-doped surface layer in silicon substrates using short-pulse boron ion implantation by the recoil method. Also calculation results for spectral detectivity and NETD of doping-spike PtSi/Si SBD detectors and HIP detectors in base of GeSi/Si heterojunction are presented.

2. Formation of heavily-doped surface layers

The barrier height for photocarriers in a metal-semiconductor structure can be reduced by producing a heavily-doped surface layer in the semiconductor. For certain parameters of the layer, an increase in the electric field in the subsurface region of the semiconductor will cause a reduction (due to the Schottky effect) of the barrier height for carriers emitting from the metal to silicon. For a substantial reduction of the metal barrier, the same type of impurity must occur in the surface nanosized layer and in the substrate, and the impurity concentration in the surface layer must be more than a hundred times as high as that found in the substrate.

Conventional boron ion implantation using CW ion sources fails to provide the parameters required for a narrow doped region. To produce a surface layer with the required parameters, the energy of accelerated boron ions must be <1 keV, and the dose must be 10^{14}–10^{16} ion cm^{-2}. Low-energy implantation like this is accompanied by different unwanted effects (sputtering of the base material, heating of the target surface exposed to an ion beam, and thermodiffusion broadening of the concentration profile). MBE is capable to produce high-purity surface layers with specified concentration of the dopant. The use of

*e-mail: vav@elefot.tsu.ru

MBE for this purpose makes possible a stepped profile of the dopant distribution in silicon. It was established that the cutoff wavelength of a Si/PtSi photodetector was increased by depositing a 1-5 nm thick film with an acceptor dopant of 5×10^{20} cm^{-3} on the surface of p-type silicon using MBE [8,9]. As pointed out above, among the drawbacks of MBE there are complex manufacturing equipment and high production cost of the structures. Recoil implantation for introduction of the impurity is performed by bombardment (normally by a rare-gas ion beam) of a thin implant layer deposited on the semiconductor surface. As the result, part of the film atoms crosses the film-substrate interface and thus penetrates the surface semiconductor layers. The bombardment causes backward sputtering, i.e., a considerable amount of the deposited film is removed.

The distribution of implanted boron in depth was estimated by using a direct analogue model approximation. The implantation profiles were calculated by the TRIM © Code using analogue modelling of spatial distributions of atoms involved in radiative mass transport. TRIM © provides realisation of a numerical method for solving the problems of passage of particles through a matter by means of statistical simulations (Monte-Carlo method). The code constructs a large number of particle trajectories in the form of polygonal lines with rectilinear segments characterizing free paths of the particles before collisions. The particle paths, the direction of motion, and the energy of a scattered particle and a recoil nucleus are random quantities described by their associated probability distribution. The slope of the concentration profile N is seen to increase with increase in the ion energy as the total yield of implanted atoms is decreased by several fold. The calculations under review show that for hydrocarbon ions, the yield is halved as the energy is increased from 30 to 200 keV, while for aluminium ions, there is a fourfold decrease in the yield for a boron film thickness of 20 nm. As the film thickness is increased, the relative number of collisions responsible for the low-energy boron atoms crossing the interface is decreased, and conversely, the fraction of boron atoms capable of penetrating deeply into the substrate is increased in proportion to the film thickness. An analysis of the obtained results shows that the yield of recoil atoms of ^{11}B is largely dependent on the energy contributed by primary ions to the region adjacent to the ^{11}B–^{27}Si interface. The boron film thickness must be chosen to be between 10 and 50 nm. At a fixed energy, the yield of the ^{11}B recoil atoms is a function of the dose of bombarded ions. All these findings have been accounted for in the design of the experiments.

A new trend in ion implantation is short-pulse implantation by high-power ion beams. Unlike continuous ion-beam implantation, the use of high-power ion beams with a current pulse duration of 10^{-7} s and average dose rate of 10^{12}–10^{13} cm^{-2} per pulse provides defect annealing in the structure of the material of the target concurrent with implantation. The instantaneous dose rate is 10^{19}–10^{20} s^{-1}cm^{-2} in an ion-flux bombardment time. The penetrating dose can be varied by varying the number of pulses and the ion current. Ion beams such as these can be generated only with an ion energy of tens of kiloelectronvolts. This renders short-pulse implantation impractical as a way of direct introduction of impurities to produce a highly-doped zone as deep as 100 Å in the subsurface region of semiconductors. However, the recoil implantation mechanism from a film deposited on the surface of the target makes possible the use of high-power ion beams for producing narrow doped layers in the subsurface region of semiconductors. Importantly, the advantages of high-current ion accelerators such as the possibility of generating ion beams of any species and of large cross sections, high dose rate, and the possibility of defect annealing concurrent with implantation are retained in this case as well.

Silicon wafers with 10-nm thick boron overlayers were irradiated by aluminium ions in a high-current pulse accelerator. The latter generated ion beams with the current density 4–10 Acm^{-2} and energy 30–50 keV. The boron film was deposited on the surface of silicon plates/wafers of KDB – 12 type by DC cathode sputtering. The as-irradiated boron film was etched in aqua-regia. The irradiated samples were subjected to thermal hydrogen annealing at 500–800°C. Boron profiles were determined by secondary ion mass spectroscopy (SIMS). The analysis was performed using a commercial device of the MS-7201M type. Its mode of operation was optimised for structures of this kind. Either pure oxygen or an oxygen-argon mixture was used as a working gas for generation of primary ion beams. The electrical parameters of silicon samples were determined by a nondestructive contact-free radiowave technique which provides high sensitivity and space resolution for materials with a specific resistance of 10^{-3}–10^{-4} Ω cm. The boron atoms were implanted into KDB-12 silicon layers/wafers by the recoil method for different irradiation doses. The number of pulses was varied between 5 and 500 (ion fluence was 2×10^{12} ions cm^{-2} per pulse). It should be noted that the qualitative pattern of the boron atom distribution in depth was the same for all irradiation doses used (10^{13}–10^{15} ions cm^{-2}). A drastic decrease was observed within 100–150 s of etching followed by a gently sloping “tail” decreasing through the entire depth studied. We believe that the slow decrease in the concentration of implanted boron atoms 5–10 nm deep (200–400 s of etching) is primarily due to the “crater” effect, i.e., to the influence of the wall composition [high boron concentration within the first 1–3 nm of the etch pit (“crater”)] on the total intensity of the secondary boron-ion component at great depths of penetration.

We have examined the form of concentration profiles in relation to the number of pulses and found no linear relation between the boron concentration in the first narrow surface layer (1-nm thick) and the irradiation dose. The absolute boron concentration in this layer was seen to saturate with increase in the number of pulses. Moreover, all investigations showed the concentration distribution profiles for

 © 2003 COSiW SEP, Warsaw

boron atoms to broaden with increase in the irradiation dose. This can primarily be attributed to heating of the surface layer exposed to high-power pulsed beams. The broadening effect is also observed in irradiated samples subjected to defect annealing. For instance, thermal annealing at 500°C for 10 min causes substantial broadening of the concentration distribution profile of boron atoms in samples exposed to 5 pulses (10^{13} ions cm^{-2}).

We have measured the electrophysical parameters of Type KDB-12 crystals subjected to implantation followed by annealing. The measurements were performed by a nondestructive contact-free radiowave technique that provides high sensitivity and spatial resolution for materials with the specific resistance $\rho = 10^{-3}$–10^{-4} Ω cm. Annealing at different temperatures is shown to increase the integral conductivity of both irradiated and nonirradiated samples to the same extent. Notably, the uniformity of distribution of ρ over the samples is improved. The results of data processing bear witness to the formation of a conducting 10–15 nm thick layer near the surface with $\rho \sim 4\times10^{-2}$ Ω cm. For a rectangular acceptor-concentration distribution over 10 nm layer thick, the hole concentration is estimated to be in the neighbourhood of 10^{18} cm^{-3}. Thus, it has been found experimentally that doping the surface silicon layer by recoil boron implantation followed by thermal annealing allows 5–15 nm thick layers to be produced on the surface of the sample. In the process, an exponential dopant distribution is observed for a surface concentration of 10^{18}–10^{20} cm^{-3}. In this case, the parameters of the doped layers can be controlled by varying the ion radiation dose and temperature and postimplantation annealing time. The implanted boron-atom distribution profile essentially depends on the total dose of incident ions and on the thickness of the boron film.

Energy-band diagrams for PtSi Schottky barriers with a heavily-doped layer have been calculated for stepped and exponential dopant distributions in the surface layer. The form of the potential Schottky barrier distribution profile is shown to be essentially dependent on the highly-doped surface layer parameters. Formation of highly-doped surface layers by molecular-beam implantation or recoil implantation techniques provides a means for changing energy-band diagrams for Si/PtSi Schottky barriers and reducing the potential barrier by ~0.15 eV. This corresponds to an ~8 μm increase in the cutoff wavelength Schottky photodetectors [12–14].

3. Spectral detectivity of SBD and HIP detectors

In this part we consider the dependencies of threshold characteristics (spectral detectivity and NETD) of PtSi/Si SBD detectors and GeSi HIP detectors versus cutoff wavelength and discuss the condition of realisation of BLIP-regime in SBD detectors operated in middle wavelength infrared (MWIR) spectral range (3–5 μm) and HIP detectors operated in long wavelength infrared (LWIR) spectral range at background temperature of 300 K.

The spectral detectivity of HIP-detectors in case of limitation of shot noise of dark current and background current can be written as

$$D_{\lambda}^{*}(\lambda) = \frac{C_1 \lambda^2 \left(\frac{1}{\lambda} - \frac{1}{\lambda_c}\right)^2}{\sqrt{2q\left(A^{**}T^2 \exp\left(-\frac{1.24q}{\lambda_c kT}\right) + C_3 C_1 \sin^2\theta \int_{\lambda_1}^{\lambda_2} \frac{\left(\frac{1}{\lambda} - \frac{1}{\lambda_c}\right)^2}{\lambda^3\left(\exp\left(\frac{C_2}{\lambda T_b}\right) - 1\right)} d\lambda\right)}}, \quad (1)$$

where q is the electron charge, T is the detector's temperature, T_b is the background temperature, A^{**} is the effective Richardson constant, λ_c is the cutoff wavelength of detector, λ is the working wavelength, θ is the half of aperture angle, C_1 is the factor of emission in eV^{-1}, $C_2 = 1.43\times10^4$ μm/K, $C_3 = 37372$ A μm^{4}cm^{-2}eV. For SBD detectors normally $C_1 = 0.2$ eV^{-1}, for HIP detectors C_1 varies from 0.1 to 1.4 eV^{-1}. Typical value of A^{**} is 3.7–10 A/cm^{2}K^2.

Formation of surface heavily-doped layer lead to increase in cutoff wavelength, quantum efficiency in spectral range 3–5 μm and, hence, to the change of threshold char-

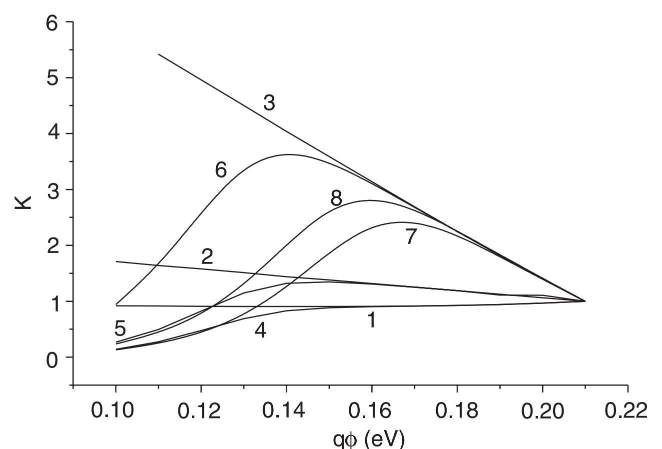

Fig. 1. Dependency of the factor K versus barrier height on PtSi/p-Si interface at $\lambda = 3$ μm (curves 1, 4), 4 μm (curves 2, 5), 5 μm (curves 3, 6–8); $2\theta = 180°$, $T = 273$ K (curves 1–7) and 300 K (curve 8); in case of BLIP (curves 1–3) and in case of account of dark current at the detector temperature of 80 K (curves 4–8); curves 4–6 at A^{**} = 0.2 A/(cmK)^2 and curves 7, 8 at A^{**} = 10 A/(cmK)^2.

acteristics. The change of threshold properties in spactral range 3–5 μm can be characterised by the coefficient K, which is equal to the relation of the spectral detectivity SBD with the cutoff wavelength λ_{C1} to the spectral detectivity SBD with the cutoff wavelength λ_{C0}

$$K = \frac{D^*_{\lambda 1}(\lambda)}{D^*_{\lambda 0}(\lambda)} = \frac{\left(1 - \frac{\lambda}{\lambda_{C1}}\right)^2}{\left(1 - \frac{\lambda}{\lambda_{C0}}\right)^2} \sqrt{\frac{C_3 C_1 \sin^2\theta \int_{\lambda_1}^{\lambda_2} \frac{\left(\frac{1}{\lambda} - \frac{1}{\lambda_{C0}}\right)^2}{\lambda^3} \frac{1}{\exp\left(\frac{C_2}{\lambda T_b}\right) - 1} d\lambda + A^{**} T^2 \exp\left(-\frac{1.24q}{\lambda_{C0} kT}\right)}{C_3 C_1 \sin^2\theta \int_{\lambda_1}^{\lambda_2} \frac{\left(\frac{1}{\lambda} - \frac{1}{\lambda_{C1}}\right)^2}{\lambda^3} \frac{1}{\exp\left(\frac{C_2}{\lambda T_b}\right) - 1} d\lambda + A^{**} T^2 \exp\left(-\frac{1.24q}{\lambda_{C1} kT}\right)}}. \quad (2)$$

Figures 1 and 2 show the calculated dependencies of spectral detectivities of HIP detectors on wavelength at various cutoff wavelengths and dependencies of the factor K on barrier heights.

As followed from Figs. 1 and 2, the optimal spectral detectivities of SBD detectors at various working wavelengths are observed at various cutoff wavelengths. The spectral detectivity of heavily doped surface nanolayer, created by short-pulse recoil implantation of boron, is equal to 3×10^{10} cmHz$^{0.5}$W^{-1} at working wavelength 3 μm and cutoff wavelength 8 μm (10^{10} cmHz$^{0.5}$W^{-1} at working wavelength 5 μm and cutoff wavelength 8 μm). The spectral detectivity at the formed surface heavily doped nanolayer decreased in short wavelength part of MWIR windows due to increased dark current and this detectivity increased in long wavelength part of MWIR windows due to increased emission efficiency.

We calculated also spectral dependencies of detectivity of HIP detectors in base of heterojunction GeSi/Si on cutoff wavelength (Figs. 3 and 4). The cutoff wavelength of HIP detectors varied in broad range 3–30 μm by change of Ge and B content in GeSi. The HIP detectors are attractive for application in LWIR spectral region 8–12 μm. As followed from Figs. 3, 4, the spectral detectivity of HIP detectors in first increased at increase in cutoff wavelength and later decreased due to increase in dark current. The spectral detecivity of HIP detectors is equal to 8×10^9 cmHz$^{0.5}$W^{-1} at working wavelength 8 μm and cutoff wavelength 12 μm (2×10^9 cmHz$^{0.5}$W^{-1} at working wavelength 10 μm and cutoff wavelength 12 μm). The spectral detectivity of HIP-detectors at increased cutoff wavelength decreases in short wavelength part of LWIR windows due to increased dark current and increase in long wavelength part of LWIR windows due to increased emission efficiency. Thus, increase in cutoff wavelength of SBD and HIP detectors at detection in MWIR and LWIR spectral range at background temperature near 300 K leads to non-monotone change of spectral detectivity of these detectors due to change of emission efficiency and dark current.

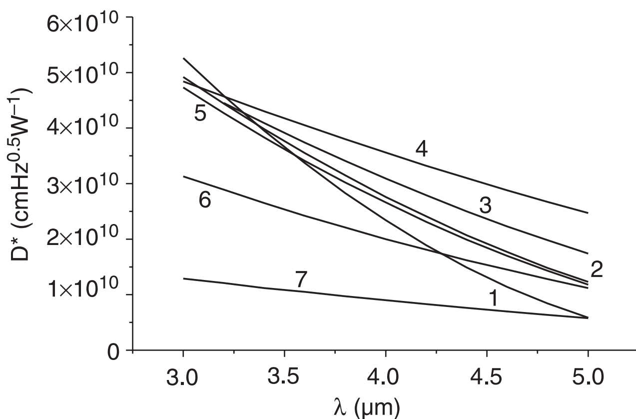

Fig. 2. Spectral detectivity of PtSi/p-Si detectors with hemispherical aperture at cutoff wavelength 6, 7, 8, and 10 μm for the case of BLIP at background temperature of 273 K – curves 1–4, respectively; at the cutoff wavelength 7, 8, 9 μm with dark current – curves 5–7, respectively.

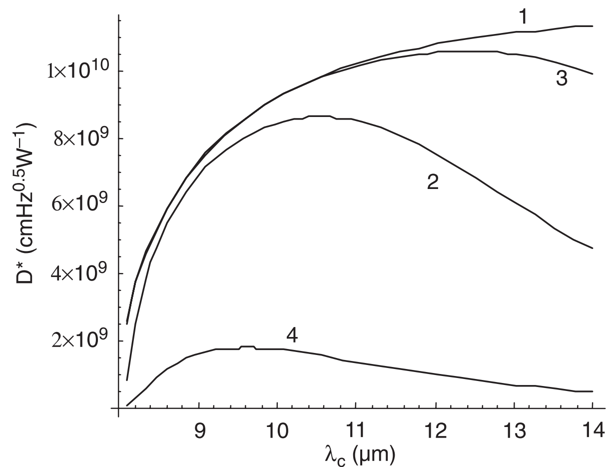

Fig. 3. Dependencies of spectral detectivities at working wavelength of 8 μm on cutoff wavelength HIP detectors at 2θ = 180° and T_b = 300 K without dark current (C_1 = 1.4 eV^{-1}, A^{**} = 3.7 A/cm^{2}K^2, T = 70 K, curve 1), with dark current (C_1 = 1.4 eV^{-1}, A^{**}= 3.7 A/cm^{2}K^2, T = 60 K, curve 2), (C_1 = 1.4 eV^{-1}, A^{**}= 3.7 A/cm^{2}K^2, T = 70 K, curve 3), (C_1 = 0.2 eV^{-1}, A^{**} = 8.4 A/cm^{2}K^2, T = 70 K, curve 4).

 © 2003 COSiW SEP, Warsaw

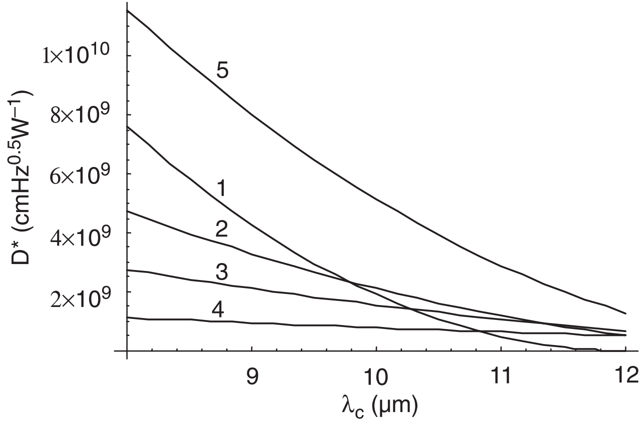

Fig. 4. Spectral dependencies of detectivity of HIP detectors assuming to background photocurrent and dark current at $2\theta = 180°$ for various cutoff wavelengths (12, 14, 16, 20 μm – curves 1–4, respectively), and without dark current at λ_c = 14 μm (curve 5) (C_1 = 1.4 eV^{-1}, A^{**} = 3.7 A/cm^{2}K^2, T_b = 300 K, T = 70 K).

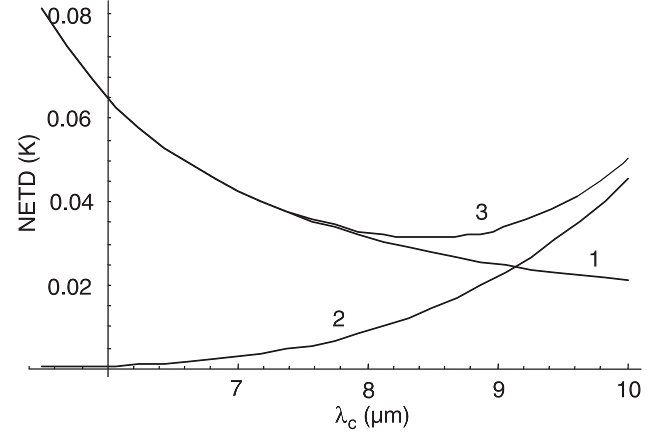

Fig. 5. Dependencies of NETD from cutoff wavelength of SBD detectors (C_1 = 0.2 eV^{-1}, A^{**}= 8.4 A/cm^{2}K^2) at detector temperature 70 K, F/2 aperture, background temperature 300 K, accumulation time 10 ms and element size 30 μm at assuming only dark current (curve 1), assuming only background photocurrent (curve 2), and assuming background and dark current (curve 3).

4. NETD of SBD and HIP detectors

The main threshold parameter of FPA is NEDT. The NETD of SBD and HIP detectors for limitation threshold characteristics of detector noise in spectral range ($\lambda_1 - \lambda_c$) [λ_1 = 8 μm] can be written as

$$NETD = \frac{(4F^2+1)\sqrt{\dfrac{2q}{A_d\tau}\left(A^{**}T^2\exp\left(-\dfrac{1.24q}{\lambda_c kT}\right)+C_3C_1\sin^2\theta\displaystyle\int_{\lambda_1}^{\lambda_c}\dfrac{\left(\dfrac{1}{\lambda}-\dfrac{1}{\lambda_c}\right)^2}{\lambda^3\left(\exp\left(\dfrac{C_2}{\lambda T_b}\right)-1\right)}d\lambda\right)}}{\displaystyle\int_{\lambda_1}^{\lambda_c}\dfrac{C_1C_2C_3\left(\dfrac{1}{\lambda}-\dfrac{1}{\lambda_c}\right)^2}{\lambda^4T_b^2\sqrt{2q}\left(\exp\left(\dfrac{C_2}{\lambda T_b}\right)-1\right)}d\lambda}, \tag{3}$$

where A_d is the detector area and is τ the accumulation time.

Figure 5 shows the dependencies of NETD SBD detectors with surface heavily doped layer on cutoff wavelength at detector temperature 70 K, F/2 aperture and background temperature 300 K for C_1 = 0.2 eV^{-1} and A^{**} = 8.4 A/cm^{2}K^2. As followed from Fig. 5, the NETD at increased cutoff wavelength of SBD in first decreased and later increased due to influence of change of dark current and quantum efficiency. In Fig. 6, the dependencies of NETD on cutoff wavelength at A^{**} = 0.2 A/cm^{2}K^2 are shown. From this figure, it followed, that creation of surface heavily-doped layer allows the NETD to be decreased from 6.5 mK at cutoff wavelength 5.5 μm to 3.5 mK at cutoff wavelength 8 μm. For smaller value of the Richardson constant, the NETD at cutoff wavelength 10 μm equals 2 mK.

We assume for calculations, the accumulation time equal to 10 ms and detector size 30 μm. In MWIR region, the accumulation time is potentially larger than in LWIR region and threshold characteristics of SBD can be improved. Figure 7 shows the dependencies of NETD HIP detectors in base of GeSi/Si on cutoff wavelength at the detector temperature 60 K, F/2 aperture and the background temperature 300 K for C_1 = 0.2 eV^{-1} and A^{**} = 4.4 A/cm^{2}K^2. As followed from Fig. 7, the NETD of HIP detectors at cutoff wavelength of 10.5 μm is 11 mK.

Figure 8 shows the dependencies of NETD stacked HIP detectors on cutoff wavelength at detector temperature 70 K, F/2 aperture and background temperature 300 K for C_1 = 1.4 eV^{-1} and A^{**} = 3.7 A/cm^{2}K^2. As followed from Fig. 8, the NETD of this stacked detector at 70 K is limited by dark current at any cutoff wavelength. In this case the minimal NETD was 7 mK at cutoff wavelength 11 μm. The calculations show that the surface heavily-doped layer in PtSi/Si created by short-pulse recoil implantation of boron can improve NETD to 3.5 mK at cutoff wavelength 8 μm.

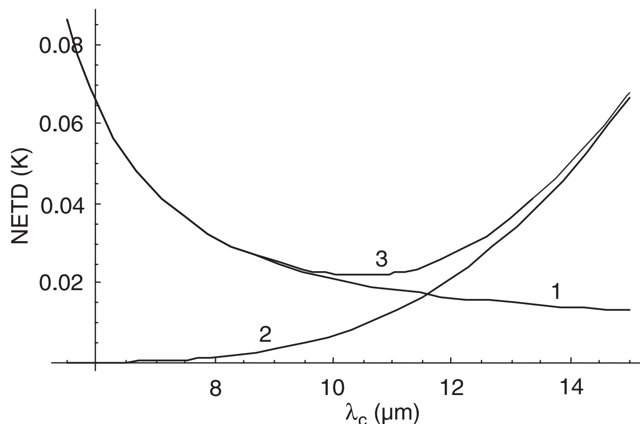

Fig. 6. Dependencies of NETD on cutoff wavelength of SBD detectors (C_1 = 0.2 eV^{-1}, A^{**}=0.2 A/cm^{2}K^2) at detector temperature 70 K, F/2 aperture, background temperature 300 K, accumulation time 10 ms and element size 30 μm assuming only dark current (curve 1), assuming only background photocurrent (curve 2), and assuming background and dark current (curve 3).

5. Conclusions

We established experimentally that creation of surface heavily-doped layer in silicon of PtSi/Si SBD using short-pulse recoil implantation of boron allows to receive the surface layer with exponential distribution of impurity at surface concentration of boron 10^{18}–10^{20} cm^{-3}.

Energy-band diagrams for PtSi Schottky barriers with a heavily-doped layer have been calculated for stepped and exponential dopant distributions in the surface layer. Formation of highly-doped surface layers by molecular-beam implantation or recoil implantation techniques provides a means for changing energy-band diagrams for Si/PtSi Schottky barriers and reducing the potential barrier by ~0.15 eV. So, the creation of surface layer using recoil implantation allows increasing cutoff wavelength of SBD to 8 μm.

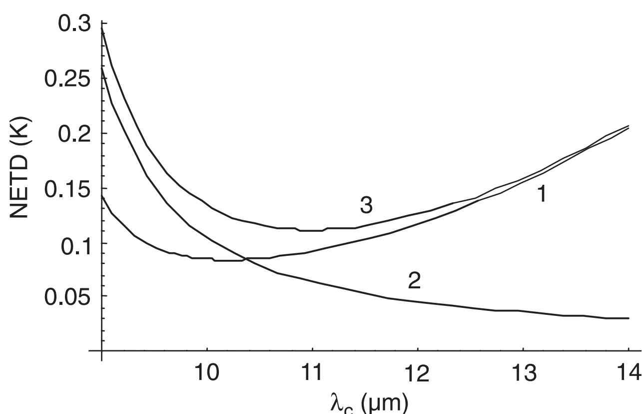

Fig. 7. Dependencies of NETD on cutoff wavelength of HIP detectors (C_1 = 0.2 eV^{-1}, A^{**}=4.4 A/cm^{2}K^2) at detector temperature 60 K, F/2 aperture, background temperature 300 K, accumulation time 10 ms and element size 30 μm at assuming only dark current (curve 1), assuming only background photocurrent (curve 2), and assuming background and dark current (curve 3).

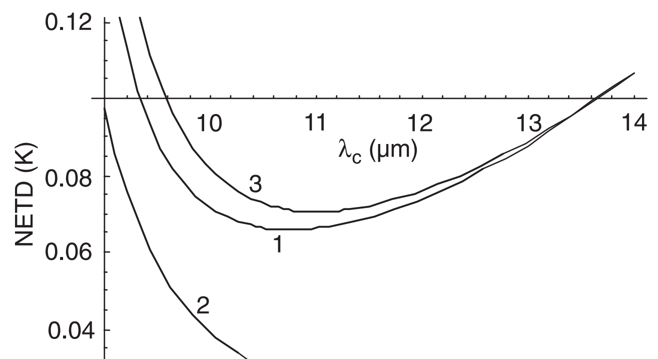

Fig. 8. Dependencies of NETD on cutoff wavelength of HIP detectors (C_1 = 1.4 eV^{-1}, A^{**} = 3.7 A/cm^{2}K^2) at detector temperature 70 K, F/2 aperture, background temperature 300 K, accumulation time 10 ms and element size 30 μm assuming only dark current (curve 1), assuming only background photocurrent (curve 2), and assuming background and dark current (curve 3).

The dependencies of spectral detectivities and NETD SBD and HIP detectors on cutoff wavelength have been calculated for various conditions of infrared detection. The expression for NETD and spectral detectivity of HIP and SBD detectors are similar due to similar mechanism of detection. It is shown that threshold characteristics of these detectors are limited by shot noise due to dark and background current. The spectral detectivity and NETD of HIP and SBD detectors are non-monotone varied with increase in cutoff wavelength due to the change in dark current and spectral quantum efficiency. The creation of surface layer used by recoil implantation can improve NETD of SBD detectors to 3.5 mK at cutoff wavelength 8 μm from 6.5 mK at typical 5.5 μm cutoff wavelength.

References

1. A. Rogalski, *Infrared Detectors*, Chapter 10, Gordon Press, London, 2000.
2. R. Breaiter, W. Cabanski, and R. Koch, "Focal plane arrays: MCT, quantum wells, PtSi", *Proc. SPIE* **3436**, 359–374 (1998).
3. V.G. Ivanov, V.I. Panasenkov, and G.V. Ivanov, "Photocarriers generation processes in Schottky barriers and possibilities to control the value and spectral dependence of quantum efficiency in an IR SB CCD", *Proc. SPIE* **3819**, 143–148 (1999).
4. P.J. Sauer, F.V. Shallcross, and F.L. Hsueh, "640×480 MOS PtSi IR sensor", *Proc. SPIE* **1540**, 285–296 (1991).
5. L.R. Hudson, H.F. Tseng, and W.L. Wang, "PtSi infrared area array utilising MOS/CTD readout", *Proc. SPIE* **819**, 262–267 (1987).
6. J.M. Shannon, "Increasing the effective height of a Schottky barrier using low energy ion implantation", *Appl. Phys. Lett*. **25**, 75–77 (1974).
7. J.M. Shannon, "Reducting the effective height of a Schottky barrier using low-energy ion implantation", *Appl. Phys. Lett*. **24**, 369–371 (1974).
8. T.L. Lin, J.S. Park, and T. George, "Doping-spike PtSi Schottky infrared detectors with extended cutoff wavelength", *Appl. Phys. Lett*. **62**, 3318–3320 (1993).

 © 2003 COSiW SEP, Warsaw

9. T.L. Lin, J.S. Park, and S.D. Gunapala, “Tailorable doping-spike PtSi infrared detectors fabricated by Si molecular beam epitaxy”, *Jpn. J. Appl. Phys.* **33**, 2435–2438 (1994).
10. T.L. Lin, A. Ksendzov, S.M. Dejewski, E.W. Jones, R.W. Fathauer, T.N. Krabach, and J. Maserjian, “SiGe/Si heterojunction internal photoemission long-wavelength infrared detectors fabricated by molecular beam epitaxy”, *IEEE Trans. Electron Dev.* **38**, 1141–1144 (1991).
11. H. Wada, M. Nagahima, and K. Hayashi, “512×512 element GeSi/Si heterojunction infrared FPA”, *Proc. SPIE* **3698**, 584–595 (1999).
12. A.V. Voitsekhovskii, A.P. Kokhanenko, A.G. Korotaev, and S.N. Nesmelov, “The photoelectric characteristics of a PtSi/Si barrier with boron heavily-doped nanolayer”, *Proc. SPIE* **4413**, 387–391 (2001).
13. A.V. Voitsekhovskii, A.P. Kokhanenko, A.G. Korotaev, and N.S. Nesmelov “Modification of parameters of silicon Shottky barriers using powerful ion irradiation”, *Proc. 1st Int. Congress on Radiation Physics, High-Current Electronics, and Modification of Materials* **3**, Tomsk, 362–365 (2000).
14. A.V. Voitsekhovskii, A.P. Kokhanenko, and A.D. Korotaev “Recoil implantation of boron in silicon for modification of parameters of silicon Schottky detectors”, *Proc. SPIE* **3881**, 274–279 (1999).

ANNOUNCEMENT and CALL FOR PAPERS

Submit your abstract to this new European meeting

26–30 April 2004
Strasbourg, France

Science • Research • Engineering
Technology • Applications • Commercialization

Present your research and be a part of this unique European event. Photonics Europe will bring together global leaders from all areas of optics/photonics research, development, and commercialization.

Photonics Europe will address the toughest issues facing optical and photonics technology developers today.

Present your research paper in these topical areas:

- Lasers
- Biophotonics
- Optoelectronics
- Nano-Photonics
- Materials
- Metrology
- Sensing
- Micro-Optics
- Packaging
- Micromachining

Plus:

- Special Hot Topics Session

Come to Strasbourg for science and engineering, but stay the week and enjoy the Photonics Hot Topics, 15 cross-disciplinary conferences, an extensive business program, a new European exhibition, and of course the superb Alsatian dining, where new friends and new ideas are just a part of the menu.

Plan now to participate and present your research.

Conferences | spie@spie.org | Tel: +1 360 676 3290

© 2003 COSiW SEP, Warsaw